Effects of Wind Angle on the Distribution of Highway Pollutants (revision 9.29.20)

QUINTIN D. SEFTON[1,2] AND JONATHAN T. STEFFENS[2]

[1] Department of Mathematics, Lafayette College, Easton, PA 18042, United States
[2] Department of Mechanical Engineering, Lafayette College, Easton, PA 18042, United States

KEY WORDS

Roadway Pollution
Pollution Dispersion
Computational Fluid Dynamics (CFD)
Wind Angles
Noise Barriers

seftonq@lafayette.edu

ABSTRACT

As our world becomes more and more industrialized, we see pollution becoming a bigger and more pressing threat to human health and wildlife. Specifically, the numerous roadways and the pollution created by cars and trucks each year is of concern. This research investigated how these pollutants come off of these roadways, and then make their way into neighboring communities. This research investigated how different wind angles affect the distribution of these highway pollutants using the CFD software ANSYS Fluent. It was found that at larger wind angles, there is more concentrated values of emission gasses, and that 50 degrees is a major angle in which these distributions change shape. This research can be used to help people design and organize community locations and homes near highways to build a safer future.

1. INTRODUCTION

The percentage of people living in urban environments is expected to grow from approximately 79% in the United States in 2000, to 83% in 2020, to an expected 89% in 2050 (United Nations, 2019). As more research is done on the impacts of pollution on living in urban environments, people are starting to notice how impactful specifically roadway pollution can be to humans. Hoek et al. (2002) found that the motility risk is 41% higher for people living within 100m of major roadways. Many other studies have shown health problems in people directly correlated with roadway pollutants such as stunted lung development in children, large increases in Coronary Heart Disease (CHD), and general asthma development and increasing asthma severity (Carla Truax et al., 2012; Wen Qi Gan et al., 2010; Michael L. Anderson, 2015; American Lung Association, 2020). Not only this, but it has also been shown that this impact is seen with both long-term and short-term exposure to roadway pollutants (Carla Truax et al., 2012). A major reason these emissions are so harmful is due to the tiny nature of the particles. The human immune system cannot detect these tiny particles and thus, the immune system does not defend against them (American Lung Association, 2020). Therefore, it is crucial to understand how we can limit these effects to our health and to understand what can be done to decrease pollution risk.

It has been shown in numerous papers that the barriers originally used to stop noise pollution off of highways, noise barriers, are doing a remarkable job to decrease the concentration of air pollutants distributed from highways as well (Steffens et al., 2014; Balfauf et al., 2008; Huertas et al., 2019; Reiminger et al., 2020; Wang and Wang, 2019). Recent research has investigated the impact of many different aspects of these barriers such as barrier height, barrier shape (Wang and Wang 2019), types of barrier configurations (Steffens et al., 2014), atmospheric temperature and atmospheric stability conditions (Reiminger et al., 2020) and much more. Only two research papers have addressed how wind angle affects these distributions and they used real life highway and sensor data to do so. These research papers had inconsistent and inconclusive results likely due to the inability to control the many independent variables such as temperature, initial concentration field, and wind speed (Kim et al., 2015; Venkatram et al., 2013). Although their research data was valuable in that they collected real world data, the aim of this research is to understand and expand the knowledge of how wind angle affects pollution dispersion using a tool that can keep independent variables constant: Computational Fluid Dynamics (CFD). More specifically, this research utilized Fluent from ANSYS Workbench.

CFD was used to understand more generally the relationship between wind angle and distribution of pollutants. This research designed a highway with a noise barrier and applied variable wind angles to determine how the distribution of pollutants is affected downwind. This research seeks to find if there is a relationship present between wind angle and concentration of highway pollutants downwind of a noise barrier. Different wind angles were compared in an attempt to determine whether there is a function that relates wind angle to pollution distribution and to determine whether a critical angle can be identified for which pollutants increase or decrease significantly. This could then lead to design criteria for the better and safer placement of homes in the future.

2. MODEL SETUP

A. Governing Equations and Model Selection

This research paper utilized the Computational Fluid Dynamics (CFD) software Fluent from ANSYS Workbench, a reliable and widely used source of CFD program (Steffens et al., 2013; Reiminger et al., 2020; Wang and Wang, 2019) and provides repeatable results that can be modified or investigated further in later research. Selecting the correct turbulence model in Fluent is crucial as the different flow software models have specific uses and will yield differing results based on small changes. For modeling air roadway dispersion, many models have been used in the past such as the Large Eddy Simulation (LES), with the Smagorinsky-Lilly subgrid model (as it models the large and small eddies in the atmosphere well) (Steffens et al., 2013; Steffens et al., 2014), the RNG $k-\epsilon$ model (Reiminger et al., 2020), the realisable $k-\epsilon$ model (Wang and Wang, 2019; Hagler et al., 2011), and many more.

This research decided to choose one of the three Reynolds-averaged Navier-Stokes (RANS) $k-\epsilon$ models, RNG, realizable, and standard, as they are very similar to each other and widely used by most fluent highway pollutant dispersion papers. This research used the realizable $k-\epsilon$ model with a Schmidt Number of 0.7 as Hagler et al. (2011) and Wang and Wang (2019) made many notable concurrences with the $k-\epsilon$ realizable model being the closest to their wind tunnel data, and Reiminger et al. (2020) and Tominaga and Stathopoulos (2007) found that a Schmidt Number of 0.7 in the realizable model most accurately modeled what was seen with their wind tunnel data.

The following equations are used in the CFD software for (1) continuity, (2) momentum, and (3) energy (as noted by Reiminger et al. 2020):

$$\frac{\partial \rho}{\partial t} + \nabla(\rho u) = 0 \tag{1}$$

$$\rho\left(\frac{\partial u}{\partial t} + u\nabla u\right) = -\nabla p + \nabla\left(2\mu_{\text{eff}}D(u)\right) - \nabla\left(\frac{2}{3}\mu_{\text{eff}}(\nabla u)\right) + \rho g \tag{2}$$

$$\frac{\partial \rho e}{\partial t} + \nabla(\rho u e) + \frac{\partial \rho K}{\partial t} + \nabla(\rho u K) + \nabla(u p) = \nabla(\alpha_{\text{eff}}\nabla e) + \rho g u \tag{3}$$

where u is velocity $[ms^{-1}]$, ρ is the density $[kgm^{-3}]$, p is pressure $[kgm^{-1}s^{-2}]$, e is thermal energy $[m^2s^{-2}]$, g is the acceleration due to gravity $[ms^{-2}]$, μ_{eff} is effective viscosity $[kgm^{-1}s^{-1}]$, α_{eff} is effective thermal diffusivity $[kgm^{-1}s^{-1}]$, and where $D(u)$ is the rate of strain tensor given in (5), and K is the kinetic energy given in (6) $[m^2s^{-2}]$:

$$D(u) = \frac{1}{2}\left[\nabla u + (\nabla u)^T\right] \tag{4}$$

$$K \equiv \frac{|u|^2}{2} \tag{5}$$

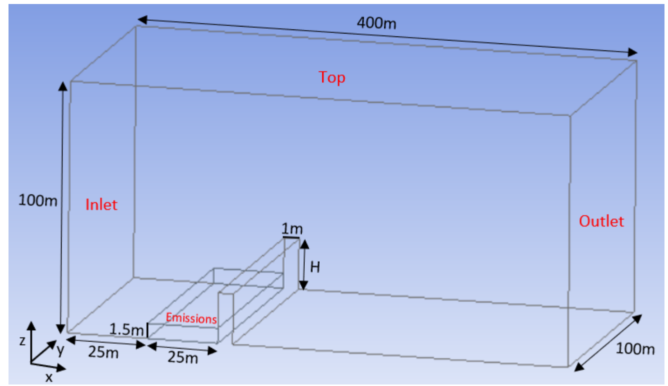

Fig. 1. Sketch of the geometry used with H=5m or H=3m (not to scale).

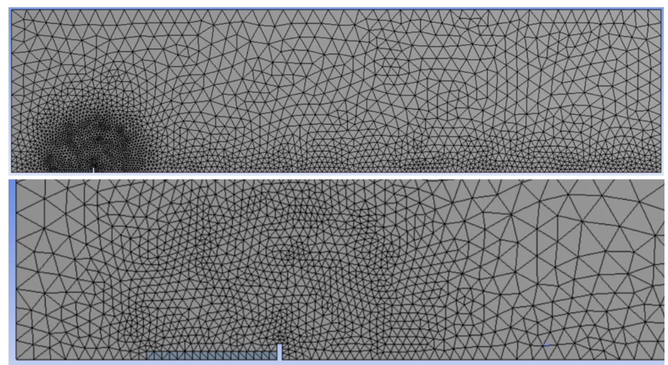

Fig. 2. A side view of the mesh for the 3m barrier height

B. Geometry and Mesh

The geometry used in this experiment simulated the full scale 1:1 model, with a 100m by 100m enclosure, 400m long to allow for recirculating areas and enough space to determine how far the pollution emissions would travel. To simulate a sound barrier, a 100m long, H tall, and 1m thick wall 50m from the inlet is used. This height, H, will be the reference length of either 5m or 3m in the two cases presented. The highway is adjacent to the wall with a 25m width and spans the 100m. Also, there is 25m of ground upwind of the highway which allows for full wind development (Fig. 1).

The mesh was designed to be more refined around the wall, the ground, and near where the inlet of the pollution gasses would be introduced because the mesh needs to be refined near areas of largest change. This mesh was created by using the automatic meshing process along with sizing parameters on the wall and ground to insure the refinement needed. The mesh had a total of 508752 elements for the 5m barrier height and 478389 elements for the 3m barrier height (Fig. 2).

With the restriction of the student version of ANSYS Fluent having a limit to the number of cells and elements (512,000) this was a good amount of elements and resulted in consistent converging results.

C. Setup and Boundary Conditions

The boundary conditions on the geometry were very important to ensure that the system behaved correctly and similar to the real world. The first major aspect of boundary conditions was the inlet conditions, more specifically the velocity profile, and the k and ϵ of the inlet conditions.

A power law profile is often employed for its ability to abide by the boundary condition of zero velocity at the ground level, and its ability to closely model the wind speed as a function of altitude (Sen et al., 2012; Touma, 1977; Wang and Wang, 2019). The power law profile equation can be seen in equation 6:

$$U(z) = U_1 \left(\frac{z}{Z_1} \right)^n \quad (6)$$

where n is typically about $1/7$, Z_1 is a reference height $[m]$, U_1 is the velocity at that reference height $[ms^{-1}]$, and $U(z)$ is the velocity $[ms^{-1}]$ as a function of the height z $[m]$. However, it has been noticed in more recent research that this velocity profile does not do as good of a job modeling the velocity in the range of intrest of about 5-100m off of the ground. Instead, many researchers have used variations of the log profile (Reiminger et al., 2020; Steffens et al., 2013; Steffens et al., 2014) which has the form of equation 7:

$$U(z) = u^* \frac{1}{\kappa} ln \left(\frac{z-d}{z_1} \right) \quad (7)$$

where κ is the von Kármán constant ($\kappa \approx .41$), u^* is the friction velocity $[ms^{-1}]$, d is the displacement height $[m]$ (sometimes taken to be 0m as in Reiminger et al., 2020, z_1 is the roughness height $[m]$, and z is the altitude $[m]$.

When deciding the velocity profile, it seemed preferable to use the log profile because of its better consciences with the observed real world wind profile at around 5-100m suggested by Reiminger et al., 2020. However, the log profile will be changed slightly so that the boundary condition of a velocity of $0ms^{-1}$ is reached at the ground similar to the power law profile. This will avoid the negative infinity velocity that would appear in the log profile resulting in unrealistic circulation events. This lead to the velocity profile being a continuous piecewise function that has both parts of the velocity profiles shown in equation 8:

$$U(z) = \begin{cases} U_1 \left(\frac{z}{Z_1} \right)^n & z \leq 2m \\ u^* \frac{1}{\kappa} ln \left(\frac{z}{z_1} \right) & z > 2m \end{cases} \quad (8)$$

where $u^* = 0.3ms^{-1}$, $z_1 = 0.5m$ (Reiminger et al., 2020), and to make the curve more continuous and differentiable, the power law profile was adjusted slightly to have values of: $U_1 = 1.01ms^{-1}$, $Z_1 = 2m$, and $n = 3/7$.

The inlet conditions for the turbulence model were specified using Turbulence Kinetic Energy (TKE, k) and Turbulent Dissipation Rate (ϵ) similar to Steffens et al. 2014; Richards and Hoxey, 1993; and Reiminger et al. 2020:

$$k = \frac{1}{2} \frac{(u^*)^2}{\sqrt{C_\mu}} \quad (9)$$

$$\epsilon = \frac{(u^*)^3}{\kappa z} \quad (10)$$

where C_μ is a CFD constant taken to be 0.085.

When deciding the emission source substance that would be tracked, it was decided to look at emission gasses are being produced by cars and their engines. Elliott et al. (2012) showed that most exhaust gasses are water, carbon dioxide, carbon monoxide, sulfur oxides, nitrogen oxides and formaldehyde. Overall, it was found that CO_2 was the most significant contributor, making up the most by volume, so it was decided to use CO_2 as the emission gas for this CFD representation.

All together, the boundary conditions are summarized with table (1):

Table 1. Boundary Conditions

Name	Boundary Type	Summary
Inlet	Velocity Inlet	Log-law profile (Eqn 11 & 12)
Outlet	Outflow	Flow Weight Rating: 1
Walls	Periodic	N/A
Highway	Emission Source	.001 $kgm^{-3}s^{-1}$ CO_2
Top	Wall	Specified Shear=0 Pa
Ground	Wall	Roughness Height: .001m
		Roughness Constant: .5m
Barrier	Wall	Roughness Height: .001m
		Roughness Constant: .5m

where the user defined velocity function for the X and Y direction respectively (u and v):

$$u = cos\left(\frac{\theta\pi}{180}\right) * IF\left(z > 2m, \frac{0.3m/s}{0.41} ln\left(\frac{z}{0.5m}\right), 1.01m/s\left(\frac{z}{2m}\right)^{(3/7)}\right) \quad (11)$$

$$v = sin\left(\frac{\theta\pi}{180}\right) * IF\left(z > 2m, \frac{0.3m/s}{0.41} ln\left(\frac{z}{0.5m}\right), 1.01m/s\left(\frac{z}{2m}\right)^{(3/7)}\right) \quad (12)$$

where θ is the angle (in degrees) from the normal to the noise barrier (i.e. 0 degrees corresponds to perpendicular to the noise barrier).

The outlet was defined to be a outflow barrier condition with an outflow weight rating of 1 (just means normal outflow without and pressure differential or velocity constraints). The two walls on the side of the region were defined to be periodic boundary conditions as this would simulate what would happen in the theoretical case of an infinitely long highway and barrier which allows for full recirculation downwind of the wall. The top surface was defined to have a specified shear of 0Pa allowing the wind at high altitudes to flow freely from the inlet to the outlet without escaping or having new gasses enter. This is reasonable to have the top keep air in as it is sufficiently high enough (100m) from the highway where recirculation zones can occur and be unaffected by this zone. The ground and barrier were then defined to have a roughness height and constant shown above as to introduce some turbulence, but also to be mostly smooth surfaces. Then, the emission source emitted $0.001kg/m^3 - s$ of CO_2 which with the emission source being 100m by 25m by 1.5m, the total amount of CO_2 was $3.75kg/s$. Finally, the temperature for all inlet and outlet conditions were set to a constant $300K$.

D. Data Collection

Wind speed was varied in increments of 5 degrees from 0 to 85 degrees for the 5m barrier height case, and the 3m barrier height case separately. Each model was run until convergence and the residuals reached 10−3. The distributions of CO_2 was then noted

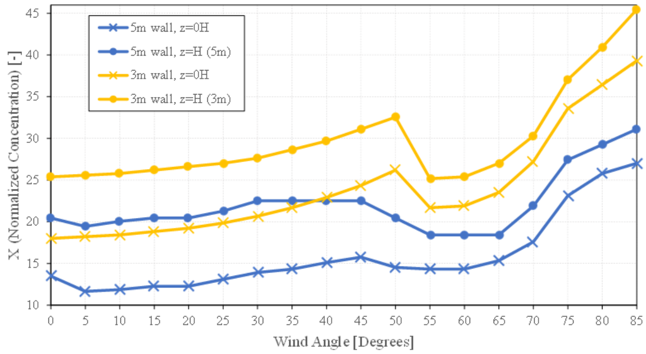

Fig. 3. Data points taken 0H downwind of the barrier at various barrier heights and wind angles.

by concentration of CO_2 at various locations as follows. Lines were created parallel to the highway, at the following locations: ground level and 0H from the barrier, ground level and 10H from the barrier, ground level and 20H from the barrier, H off of the ground and 0H from the barrier, H off of the ground and 10H from the barrier, and H off of the ground and 20H from the barrier (Note: for the 5m barrier height, 5m=H, and for the 3m barrier height, 3m=H). These lines then each took 999 data points of concentration and the average concentration along these lines was then calculated and recorded.

The distributions of CO2 were recorded and then a normalized concentration was calculated as follows (13):

$$\chi = \frac{CU_r L_x L_y}{Q} \tag{13}$$

where $U_r = 3.071 m/s$ is the reference velocity taken at 30m, $L_x = 25m$ and $L_y = 100m$ are characteristic lengths of the roadway source region, and Q=3.75kg/s is the source emission rate.

3. RESULTS AND FIGURES

The figures presented will be organized by how far CO_2 concentration measurements were taken from the wall. Then, it will be explained why it is believed that these figures make sense and try to explain and describe why the figures behave the way they do.

Fig. 3 shows all data taken 0m from the wall at ground level and at wall height off of the ground for the 2 varying barrier cases. The second figure, Fig. 4, shows the data, but taken 10H downwind from the barrier (30m and 50m for the 3m and 5m barrier case respectively). Finally, the third figure, Fig. 5, shows the data at a distance of 20H downwind from the barrier (60m and 100m).

The first thing to be noted about this data is that the concentration at any point in the 3m barrier case is always larger than that of the concentration at a similarly located point for the 5m barrier case. This makes sense as the two simulations started with the same initial emission rate of CO_2 at the emission source, but with the shorter barrier height of 3m, more CO_2 emission gas is able to make it over the wall and increase the concentration downwind of the barrier than the 5m barrier case. Another reason there is more pollutant gas measured downwind in the 3m barrier case is because in the 5m barrier case, more gas is trapped behind the barrier and still on the highway.

Another trend in these data, is that in every figure, the concentration increases as wind angle increases. More specifically, the

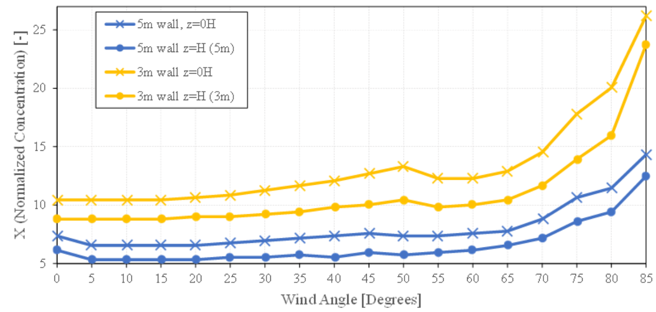

Fig. 4. Data points taken 10*H downwind of the barrier at various barrier heights and wind angles.

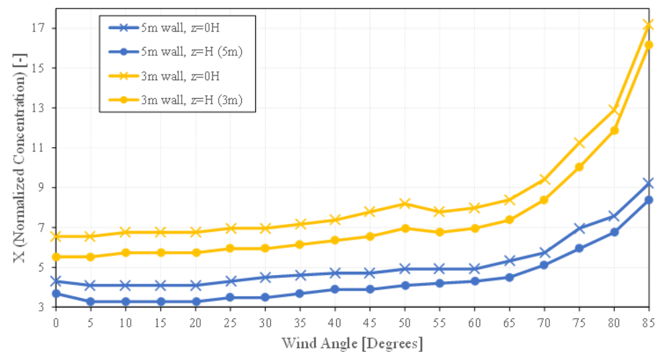

Fig. 5. Data points taken 20*H downwind of the barrier at various barrier heights and wind angles.

concentration increases drastically with wind angle after around 60 degrees. This is likely due to adjective transport being the dominant transport process for the CO_2 gas. Diffusion no longer becomes as significant and we see that the larger, more oblique wind angles result in CO_2 gas staying near the barrier while smaller, more perpendicular wind angles result in lots of adjective transport of CO_2 gas over the wall. With the more transport over the wall and diffusing downwind more with more perpendicular wind angles, we see less concentration downwind as the gas is being spread further, more thin, and therefore less concentrated.

In Fig. 6, there is Fig. 3, Fig. 4, and Fig. 5 with the x-axis replaced with cosine of the wind angle. This new x-axis is similar to perpendicular wind speed and seeing how that affects the distribution. Fig. 6 shows that as perpendicular wind speed ($cos(\theta)$) increases, we tend to see less concentration of CO_2 gas. This is congruent to what was observed in previous graphs as well, but the cosine graphs shows us the relationship that could be compared to wind speed in the future.

One thing that can be noticed in all of these graphs is that there is a clear deviation from the trend at around 50 degrees. If we look at Fig. 3, for the 3m barrier case, there is a clear, steady increase in concentration as wind angle increases from 0 to 50 degrees, and then a sharp decrease in concentration at 55 degrees. Originally, this was fairly random and did not seem to make much sense, but with some further research into the 50 degree and 55 degree case, it seems to make more sense. Below is Fig. 7 and Fig. 8 which shows the 50 degree and 55 degree case respectively. It can be clearly seen that the velocity profile is different for both of these figures. In the 50 degree case, we

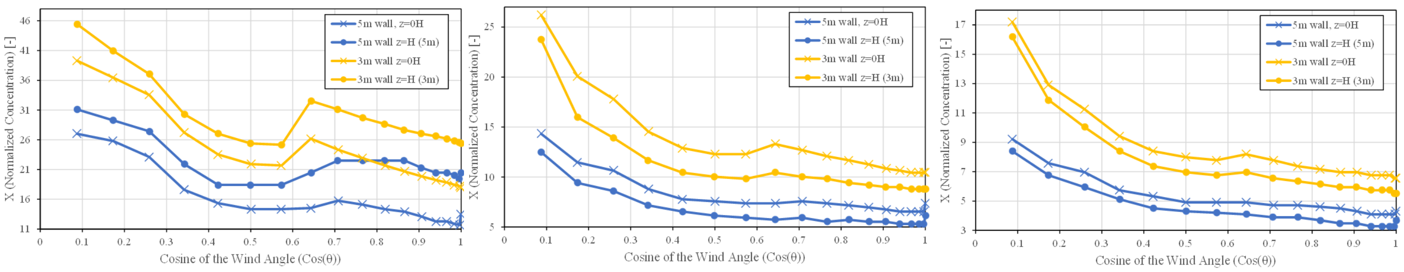

(a) Caption 1 **(b)** Caption 2 **(c)** Caption 1

Fig. 6. Caption for 3 images

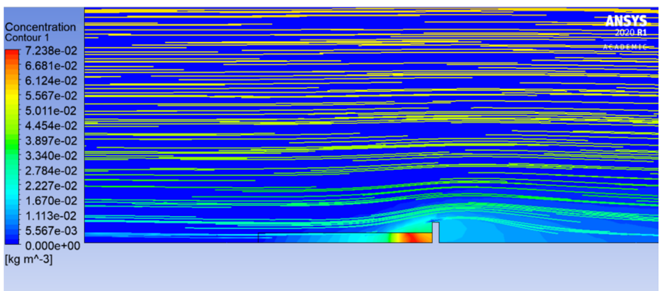

Fig. 7. 50 degree wind angle case with a 3m barrier.

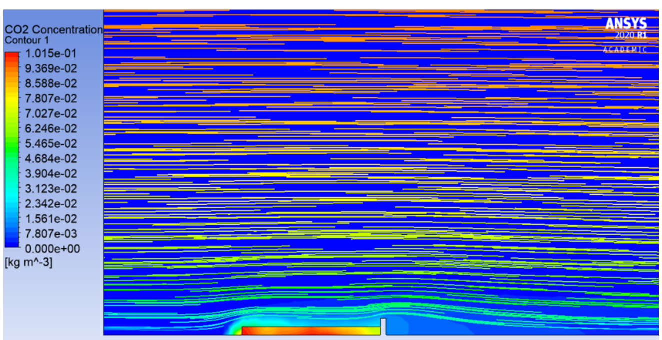

Fig. 8. 55 degree wind angle case with a 3m barrier.

see that the wind goes through the emission source and is able to pick up more CO_2 emissions. With the 55 degree case, the velocity profile shows that it does not go through the emission source and instead avoids it and in a way captures it sealing it off from being distributed further downwind past the barrier.

In smaller angles, it is seen that the wind velocity profile behaves similar to the 50 degree case by passing into the emission source section. On the other hand, the larger angles, past 55 degrees, behave similar to the 55 degree case. This tendency for smaller angles to be able to pierce through the CO_2 region, and the larger angles to trap and erode on the CO_2 region is likely why we see the disjoint nature in these two angle groups.

4. CONCLUSION

CFD software ANSYS Fluent was used to simulate how different wind angles affect the distribution of emission sources from cars, trucks, and other highway pollutants. It has been found that higher wind angles have resulted in higher concentrations at the measured locations and that there is a critical angle in which the wind velocity profile changes from interacting with the emissions greatly, to not interacting much and capturing it before the barrier. These general conclusions can be made and can possibly be considered when deciding where and how to design major roadways, barriers, and societies near roadways.

This information can be further expanded upon in many different avenues. This research could be further explored by investigating how wind angle can influence the distribution with different barrier heights, different layouts and roadway configurations, different vegetation barriers, different wind temperatures, different roughness heights, different wind stability conditions, and much more. This general knowledge that has been explored is still valuable and is in accordance with Venkatram et al. 2013 which also concluded that higher wind angles resulted in higher concentrations of emissions in his study using real roadway data that was not fully conclusive. Hopefully this paper sheds some more light into why this conclusion was shared and why that is the case which can be expanded upon further in the future.

Roadway pollution is a big problem that is often overlooked in our world today that we, as humans, need to be more aware of. The pollution created and dispersed into our world is only going to get worse unless we are able to understand how to better control it. The research being done in this area will help aid people to understand how to better design, lay out, and build a safer future for our communities and families.

5. ACKNOWLEDGMENTS

We would like to thank Professor Steffens for helping greatly with this research project, and Lafayette College of Easton, P.A. for their support.

REFERENCES

1. Wang, S., Wang, X., 2019. Modeling and analysis of the effects of noise barrier shape and inflow conditions on highway automobiles emission dispersion. Fluids 4, 151. https://doi.org/10.3390/fluids4030151.
2. United Nations, Department of Economic and Social Affairs, Population Division, 2019. World Urbanization Prospects: the 2018 Revision (ST/ESA/SER.A/420). United Nations, New York.
3. Richards, P.J., Norris, S.E., 2011. Appropriate boundary conditions for computational wind engineering models revisited. J. Wind Eng. Ind. Aerod. 99, 257–266. https:// doi.org/10.1016/j.jweia.2010.12.008.
4. Richards, P.J., Hoxey, R.P., 1993. Appropriate Boundary Conditions for Computational Wind Engineering Models Using the K-E Turbulence Model, vol. 9.
5. Hoek, G., Brunekreef, B., Goldbohm, S., Fischer, P., van den Brandt, P. A., 2002. Association between mortality and indicators of traffic-

related air pollution in the Netherlands: a cohort study. Lancet (London, England), 360(9341), 1203-1209. https://doi.org/10.1016/S0140-6736(02)11280-3
6. Truax, C, 2012. Driving Harm: Health and Community Impacts of Living near Truck Corridors.THE Impact Project Policy Brief Series. https://envhealthcenters.usc.edu/wp-content/uploads/2016/11/Driving-Harm.pdf
7. Gan, W., Tamburic, L., Davies, H., Demers, P., Koehoorn, M., Brauer, M. (2010). Changes in Residential Proximity to Road Traffic and the Risk of Death From Coronary Heart Disease. Epidemiology, 21(5), 642-649. Retrieved August 13, 2020, from www.jstor.org/stable/20788202
8. Anderson, M.L., 2015. As the Wind Blows: The Effects of Long-Term Exposure to Air Pollution on Mortality. NBER Working Paper No. 21578, JEL No. I12,Q53. http://www.nber.org/papers/w21578
9. American Lung Association 2020. Particle Pollution. Retrieved from https://www.lung.org/clean-air/outdoors/what-makes-air-unhealthy/particle-pollution
10. Steffens, J.T., Heist, D.K., Perry, S.G., Isakov, V., Baldauf, R.W., Zhang, K.M., 2014. Effects of roadway configurations on near-road air quality and the implications on roadway designs. Atmos. Environ. 94, 74-85.
11. Steffens, J.T., Wang, Y.J., Zhang, K.M., 2012. Exploration of effects of a vegetation barrier on particle size distributions in a near-road environment. Atmos. En- viron. 50, 120-128.
12. Steffens, J.T., Heist, D., Perry, S., Zhang, K.M., 2013. Modeling the effects of a solid barrier on pollutant dispersion under various atmospheric stability conditions. Atmos. Environ. 69, 76-85.
13. Baldauf, R., Thoma, E., Khlystov, A., Isakov, V., Bowker, G., Long, T., Snow, R., 2008. Impacts of noise barriers on near-road air quality. Atmos. Environ. 42 (32), 7502e7507.
14. Huertas, J.I., Prato, D.F., 2019. CFD Modeling of Near-Roadway Air Pollution. Environmental Modeling and Assessment. 10.1007/s10666-019-09666-w.
15. Reiminger, N., Jurado, X., Vazquez, J., Wmmert, C., Blond, N., Dufresne, M., Wertel, J., 2020. Effects of wind speed and atmospheric stability on the air pollution reduction rate induced by noise barriers. Journal of Wind Engineering & Industrial Aerodynamics, 200. https://doi.org/10.1016/j.jweia.2020.104160.
16. Kim, Kyung Hwan & Lee, Seung-Bok & Woo, Daekwang & Bae, Gwi-Nam. (2015). Influence of wind direction and speed on the transport of particle-bound PAHs in a roadway environment. Atmospheric Pollution Research. 1-11. 10.1016/j.apr.2015.05.007.
17. Venkatram, A., Snyder M., Isakov V., Kimbrough, S., 2013. Impact of wind direction on near-road pollutant concentrations. Atmos. Environ. 80, 248-258. https://doi.org/10.1016/j.atmosenv.2013.07.073.
18. Hagler, G., Tang, W., Freeman, M., Heist, D., Perry, S., Vette, A., 2011. Model evaluation of roadside barrier impact on near-road air pollution. Atmos. Environ. 45 (15), 2522-2530. https://doi.org/10.1016/j.atmosenv.2011.02.030.
19. Tominaga, Y., Stathopoulos, T., 2007. Turbulent Schmidt numbers for CFD analysis with various types of flowfield. Atmos. Environ. 41 (37), 8091-8099. https://doi.org/10.1016/j.atmosenv.2007.06.054.
20. Şen, Z., Altunkaynak, A., Erdik, T., 2012. Wind Velocity Vertical Extrapolation by Extended Power Law. Hindawi Publishing Corp. 2012, Article ID 178623. https://www.hindawi.com/journals/amete/2012/178623/.
21. Touma, J.S., 1977. Dependence of the Wind Profile Power Law on Stability for Various Locations, Journal of the Air Pollution Control Association, 27:9, 863-866. https://doi.org/10.1080/00022470.1977.10470503.
22. Elliot, M.A., Nebel, G.J., Rounds, F.G., 2012. The Composition of Exhaust Gases from Diesel, Gasoline and Propane Powered Motor Coaches. APCA, 5, 103-108. https://doi.org/10.1080/00966665.1955.10467686